

The kinetics and mechanisms of schwertmannite transformation to goethite and hematite under alkaline conditions

LOIS E. DAVIDSON, SAMUEL SHAW,* AND LIANE G. BENNING

School of Earth and Environment, University of Leeds, Leeds, LS2 9JT, U.K.

ABSTRACT

The transformation of schwertmannite to goethite and/or hematite in high pH solutions was studied between 60 and 240 °C using synchrotron-based, in-situ energy-dispersive X-ray diffraction (EDXRD). Powder diffraction and electron microscopy indicate that the crystallization of hematite and goethite occurred via intermediate ferrihydrite. At temperatures ≤ 80 °C goethite was the only crystallization product, while at temperatures > 80 °C goethite and hematite crystallized almost simultaneously. At temperatures ≥ 150 °C a secondary crystallization stage was observed in which goethite transformed to hematite. The activation energies of nucleation for goethite and hematite are 27 ± 1 and 25 ± 1 kJ/mol, respectively, while the activation energies of crystallization are 33 ± 1 and 28 ± 1 kJ/mol. Most of the sulfate was released from the schwertmannite during the early stages of crystallization with $< 5\%$ of the sulfate remaining associated with the solid phase after crystallization was complete. Sulfate from the initial schwertmannite retarded the dissolution of ferrihydrite, which inhibited the nucleation and the early stages of goethite formation, but did not significantly affect the later stages of goethite crystallization. At high temperatures the presence of sulfate favored the crystallization of hematite over goethite. The activation energy of crystallization for the secondary transformation of goethite to hematite is 103 ± 3 kJ/mol.

Keywords: Schwertmannite, ferrihydrite, goethite, hematite, sulfate, time-resolved, energy-dispersive X-ray diffraction

INTRODUCTION

Schwertmannite, with an idealized formula $\text{Fe}_8\text{O}_8(\text{OH})_x\text{SO}_4$, commonly forms in acid mine drainage (AMD) environments as a poorly crystalline and nanoparticulate mineral phase (e.g., Bigham et al. 1990, 1996; Childs et al. 1998; Yu et al. 1999; Jönsson et al. 2005). The oxidation of pyrite in these systems releases large amounts of ferrous iron, sulfate, and acidity into associated ground and surface water. The oxidation of ferrous to ferric iron when the waters come into contact with the atmosphere leads to the precipitation of various Fe^{3+} (oxy)hydroxides and (oxy)hydroxy-sulfate minerals. At circum-neutral pH values ferrihydrite is the dominant phase formed, schwertmannite is the most common direct precipitate from AMD waters in the pH range 2–4, and jarosite is the prevalent phase at $\text{pH} < 2$ (Brown 1971; Cravotta et al. 1999).

Characterization of natural and synthetic samples using electron microscopy has shown that schwertmannite forms spherical aggregates of up to 2 μm in size that consist of radially oriented, acicular crystals, ca. 100 nm in length and 10 nm wide (e.g., Bigham et al. 1990, 1996; Loan et al. 2004; Regenspurg et al. 2004). Based on data from both synthetic and natural samples, Bigham et al. (1990) suggested that schwertmannite has a structure similar to akaganéite ($\beta\text{-FeOOH}$) with double corner-sharing chains of $\text{FeO}_3(\text{OH})_3$ octahedra that produce square tunnels parallel to the *c* axis. These tunnels are stabilized by the presence of sulfate oxyanions, which form bidentate bridging

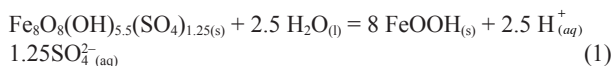
complexes with Fe^{3+} in the structure. Studies also indicate that the individual schwertmannite particles are elongated along the *c* axis of the schwertmannite structure (Bigham et al. 1990; Bigham and Nordstrom 2000). However, Loan et al. (2004) showed that the individual schwertmannite particles have a maghemite-like structure, similar to that described by Janney et al. (2001) for ferrihydrite, although within the particles there was also evidence of more disordered and amorphous regions.

Natural and synthetic schwertmannite have variable iron, sulfate, and water contents (e.g., Bigham et al. 1990, 1996; Childs et al. 1998; Yu et al. 2001, 2002) leading to a general formula that can be expressed as $\text{Fe}_8\text{O}_8(\text{OH})_{8-2x}(\text{SO}_4)_x \cdot n\text{H}_2\text{O}$, where $1 \leq x \leq 1.75$ (Bigham et al. 1994). In addition to the highly variable sulfate content, sulfate can be substituted by a range of (toxic) anions, such as arsenate (e.g., Carlson et al. 2002; Fukushi et al. 2003a, 2003b, 2004), selenate (Waychunas et al. 1995), and chromate (Regenspurg and Peiffer 2005). Schwertmannite has a high surface area (e.g., 240–320 m^2/g for synthetic and 125–225 m^2/g for natural samples; Bigham et al. 1990) and reactivity that results in a high sorption capacity for a wide variety of dissolved trace elements and contaminants (Webster et al. 1998; Jambor and Dutrizac 1998). For example, schwertmannite has been shown to effectively remove arsenic (e.g., Carlson et al. 2002; Fukushi et al. 2004), chromium (Regenspurg et al. 2005), selenium (Waychunas et al. 1995), copper, and zinc (Swedlund and Webster 2001) from solution. This efficient contaminant sequestration shows that schwertmannite can exert a significant

* E-mail: s.shaw@see.leeds.ac.uk

control on the mobility, speciation, and bioavailability of many trace contaminants present within AMD environments.

Schwertmannite has been shown to be thermodynamically unstable with respect to goethite, hematite, and jarosite. In laboratory studies, Bigham et al. (1996) showed that synthetic schwertmannite equilibrated with distilled water (pH 3.9) at room temperature transformed to goethite over a period of 543 days. This transformation reaction occurs as follows:



Experiments by Schwertmann and Carlson (2005) showed that, at room temperature, schwertmannite in equilibrium with de-ionized water adjusted to pH values between 4 and 7.2 transformed completely to goethite within 100 days. The transformation followed a first-order relationship with respect to the concentration of schwertmannite and the reaction rate was highly pH dependent, almost doubling across the pH range (i.e., low at pH 4 and high at pH 7.2). The transformation of schwertmannite to goethite has also been observed in natural environments (e.g., Jiang and Chen 2005; Gagliano et al. 2004). Based on temporal variations in mine shaft water levels, the distribution of goethite and schwertmannite within the mine-waste-rock piles and saturation/stability of schwertmannite with respect to the geochemistry of the AMD waters at the Alta Mine, Montana, Schroth and Parnell (2005) proposed a dissolution/re-precipitation mechanism for the transformation of schwertmannite to goethite in natural settings. Schwertmannite has also been observed to transform to hematite under hydrothermal conditions at 200 °C (Barham 1997), although no information about the kinetics or mechanism of this reaction is known. The sulfate content of schwertmannite (Bigham et al. 1996) and the presence of adsorbed and/or substituted contaminants (e.g., arsenate and chromate; Regenspurg et al. 2005), also play an important role in the kinetics of transformation, with the reaction rate slowing with increased sulfate and contaminant concentration.

To make accurate predictions about the stability of schwertmannite in the environment, it is important to quantify the mechanisms and the kinetics of its transformation to more crystalline iron (oxyhydr)oxide phases. However, there is a lack of detailed time-resolved observations on these reactions, therefore little quantitative kinetic and mechanistic data are available. The aim of this study was to quantify the kinetics, mechanisms, and products of schwertmannite transformation, using in-situ, time-resolved, synchrotron-based, energy-dispersive X-ray diffraction (EDXRD) combined with off-line chemical and microscopic characterization.

EXPERIMENTAL METHODS

Schwertmannite preparation and characterization

Schwertmannite was prepared at room temperature by mixing 1 L of a 100 *M* ferrous ammonium sulfate solution [prepared anaerobically using reagent-grade salts and de-oxygenated, de-ionized water (DIW)] and 1 L 33 *mM* H₂O₂ solution with the pH of both solutions adjusted to 3 using either de-gassed 1 *M* NaOH or 1 *M* HCl. After a few minutes mixing, a reddish-brown precipitate formed. The suspension was stirred continuously for 24 h. After settling, the supernatant was removed and the solid separated by filtration and washed 3 times with DIW. The washed solid product was oven dried at 40 °C and stored in a desiccator. The

synthesis product was characterized by powder X-ray diffraction (XRD) using a Philips PW1050 X-ray diffractometer (CuK α radiation), with a post sample monochromator. Analytical transmission electron microscopy (TEM) of the powdered samples was performed using a Philips/FEI CM200 field emission gun TEM operating at 197 kV, fitted with an ultra thin window energy dispersive X-ray (EDX) detector (Oxford Instruments ISIS). TEM specimens were prepared by sonicating a few milligrams of the solids in 10 mL ethanol for 10 min and then evaporating to dryness onto holey carbon coated copper TEM grids (Agar Scientific Ltd.). The effective diameter of the selected area electron diffraction (SAED) aperture at the image plane was approximately 0.18 μm .

To determine the chemical composition of the synthesis product, 200 mg of the solid phase were digested for 2 h in 100 mL of 0.25 *M* hydroxylammonium hydrochloride (made in 0.25 *M* HCl). The solution was analyzed for total iron using inductively coupled plasma optical emission spectroscopy (ICP-OES, Perkin Elmer ICP 5300 DV). The errors on the analyses were calculated as twice the relative standard deviation from certified standard solutions. The concentration of sulfate was determined by ion chromatography (IC, Dionex DX-600 ion chromatograph with an EDS50A UVD 170U detector and an Ionpac AS16 column). The elute concentration and flow rate were set such that the chloride (from HCl) and sulfate signals did not interfere with one another. The error on these analyses was calculated as twice the relative standard deviation from the mean of nine measurements (three repeat measurements of triplicate samples).

Off-line, ex-situ transformation experiments

Laboratory-based crystallization experiments were conducted at 80 and 180 °C to determine changes in solid phase mineralogy and supernatant composition during the transformation of schwertmannite. These experiments were performed using the following procedure: 2 g dry powdered schwertmannite were loaded into a Teflon-lined 20 mL steel Parr reactor containing a micro-magnetic stirrer and mixed with 10 mL of a 1 *M* NaOH solution. The reactor was placed into a heated oil bath with the temperature maintained at the desired value using a thermocouple connected to a heater unit. Several parallel experiments were performed and the reactions quenched at regular time intervals up to 6000 s by plunging the reactor into ice-cold water. The quenching step was estimated to be complete in <2 min. The contents were filtered through 0.2 μm polycarbonate filters, the pH of the supernatants measured using a pH probe calibrated with NIST certified pH buffers, and the sulfate concentration determined by IC as described above. The filtered solid products were washed three times in DIW, dried, and characterized by powder X-ray diffraction and TEM as described above.

Time-resolved, in situ EDXRD experiments

In-situ time-resolved studies of schwertmannite transformation were carried out using the EDXRD facilities on station 16.4 at the Synchrotron Radiation Source (SRS), Daresbury Laboratory, U.K. The station configuration and experimental set-up have been described in detail by Shaw et al. (2000). The transformation experiments were conducted by transferring 2 g of dry powdered schwertmannite into a PTFE liner containing a micro-magnetic stirring bar. The liner was placed in a modified steel Parr reactor, with a section of the wall milled down to permit sufficient X-ray transmission. To initiate the experiments, 10 mL of 1 *M* NaOH solution were added to the cell and the reactor was quickly sealed and placed in a pre-heated aluminum heating block fitted with four resistance heating cartridges and a thermocouple to heat and maintain constant temperature. A magnetic stirrer ensured continuous stirring of the suspension. Two slots in the aluminum block, aligned with the milled section of the reactor, allowed the white X-ray beam to pass through the apparatus and sample. Post sample collimation ensured that X-rays were diffracted solely by the contents of the cell and that there was no input from the PTFE liner or steel reactor. During experiments, the energy dispersive capabilities of the station set-up allowed the whole diffraction pattern to be collected simultaneously using three energy-sensitive solid state detectors set at fixed diffraction angles (2 θ). For data evaluation, only peaks observed on the middle detector were used because this detector recorded the most appropriate *d*-spacing range.

Experiments were carried out at temperatures between 60 and 240 °C and for each isothermal experiment diffraction patterns were collected every 1 or 2 min. The length of the experimental runs varied between 20 and 500 min, depending on observed real-time changes in specific Bragg peaks.

EDXRD data analysis

The *d*-spacings of the peaks present in diffraction patterns were calculated from the energies of the peak positions, *E*, and the angles of the detector, θ , us-

ing a modified form of Bragg's law ($E = 6.199/d\sin\theta$; Finger 1989). Peaks within individual diffraction patterns were fitted using the program XFIT (Cheary and Coelho 1992) using the Gaussian peak function to evaluate peak positions and area. The changes in peak area with time were normalized to give the degree of the reaction, α , using the following equation:

$$\alpha = \frac{I_t}{I_{\max}} \quad (2)$$

where I_t represents the peak area at a given time and I_{\max} the peak area at the end of the reaction. The normalized data as a function of time were subsequently fitted with the Johnson-Mehl-Avrami-Kolmogorov (JMAK) kinetic model (Avrami 1939, 1940; Johnson and Mehl 1939) using the following equation:

$$\alpha = 1 - e^{-k(t-t_0)^n} \quad (3)$$

where k (s^{-1}) is the rate constant for the reaction, t (s) is time, t_0 (s) is the induction time (first appearance of a peak), and n is a variable that depends on the nucleation rate, reaction mechanism, and dimensionality of growth (Hulbert 1969). Note that the rate constants calculated using Equation 2 represent conditional rate constants, because they take into account several processes occurring simultaneously (e.g., dissolution, nucleation, growth; Lasaga 1998).

Two types of reaction mechanism were considered when interpreting the value of n . The first was a surface or phase-boundary controlled mechanism, in which the reaction does not proceed fast enough to attain equilibrium at the particle-solution interface and the reaction is limited by the amount of interface available. The second assumed a diffusion, or transport controlled mechanism, in which the reaction rate is controlled by the rate of transport of reactants through the matrix to the particle surface.

The apparent activation energy of crystallization was calculated from the experiments performed at different temperatures, using the Arrhenius equation:

$$\ln k = \ln A_{(\text{cryst})} - \frac{E_a(\text{cryst})}{RT} \quad (4)$$

where A is the pre-exponential factor (s^{-1}), E_a is the apparent activation energy (kJ/mol), R is the gas constant [8.314 J/(mol·K)], and T is the absolute temperature (K). The apparent energy of nucleation was calculated using the following adaptation of the Arrhenius relationship (Kaschiev 1969):

$$\ln t_0 = \ln A_{(\text{nucl})} + \frac{E_a(\text{nucl})}{RT} \quad (5)$$

RESULTS

Schwertmannite characterization

Powder X-ray diffraction data (Fig. 1) of the schwertmannite starting material shows all eight broad diffraction peaks characteristic of schwertmannite (Bigham et al. 1990). TEM characterization (Fig. 2) showed that the schwertmannite formed aggregates 500 to 1000 nm in diameter with a characteristic "pin cushion" morphology (Bigham et al. 1990). The aggregates consisted of radially orientated elongated particles that measured 5 to 10 nm in width, and between 10 and 50 nm in length. TEM-EDX analyses confirmed that the particles consisted of iron, oxygen, and sulfur (Fig. 2). The SAED pattern from the aggregate revealed the two strongest lattice reflections, (212) and (004), for schwertmannite (Fig. 2).

Analyses of the digested starting material (data not shown) revealed a total sulfate concentration of 14.7 ± 0.6 wt% and an iron content of 42.0 ± 0.8 wt%. From these data the formula for the schwertmannite used in this study was determined to be $\text{Fe}_8\text{O}_8(\text{OH})_{4.74}(\text{SO}_4)_{1.63} \cdot n\text{H}_2\text{O}$.

Crystallization reactions

The off-line crystallization experiments resulted in the complete transformation of schwertmannite to goethite at 80 °C

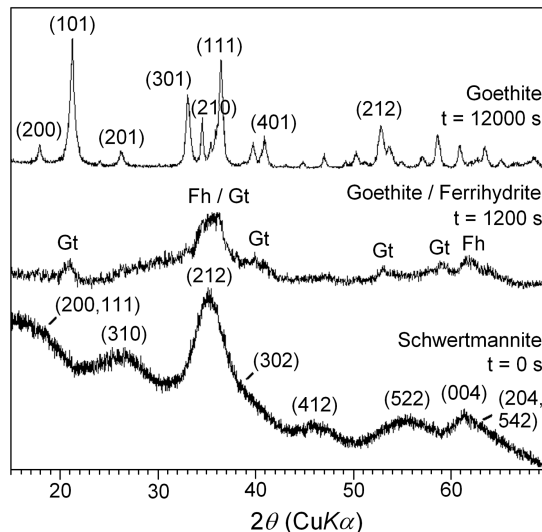


FIGURE 1. Powder X-ray diffraction patterns (offset for clarity) of the solid fractions quenched at various time frames during the transformation of schwertmannite to goethite at 80 °C; schwertmannite starting material ($t = 0$ s) (bottom pattern); two-line ferrihydrite intermediate, with minor goethite ($t = 1200$ s) (middle pattern); and pure goethite end product ($t = 12000$ s) (upper pattern). The major hkl assignments of the phases are labeled.

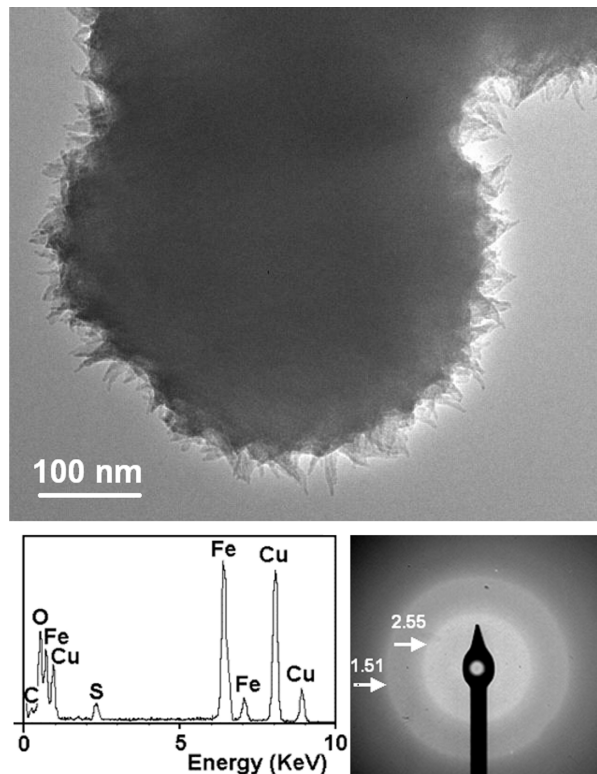


FIGURE 2. TEM image of a schwertmannite aggregate displaying typical "pin cushion" morphology. Inserts: EDX pattern of schwertmannite exhibiting iron, oxygen, and sulfur signals (the copper signals are from the copper mesh TEM grid); and a SAED pattern of the schwertmannite aggregate. The two major schwertmannite reflections, (212) and (004) are labeled with white arrows, d -spacings in angstroms.

(Fig. 1) or hematite at 180 °C (not shown) as sole end-products. An XRD pattern of a sample quenched 20 min after the start of the reaction at 80 °C (Fig. 1), showed that the 8 diffraction peaks of the initial schwertmannite were no longer present and that two broad peaks indicative of 2-line ferrihydrite and minor peaks representing goethite had appeared. The presence of ferrihydrite was also confirmed by TEM (Fig. 3a) and is shown to have formed loose aggregates of nanoparticles. SAED of these aggregate show the two diffuse rings typical of 2-line ferrihydrite, and no sulfate was detected in the EDX spectra. Goethite was associated with this intermediate ferrihydrite (Figs. 1 and

3a), but after 200 min the final solid phase was entirely goethite (Figs. 1 and 3b).

Data from the time-resolved, in-situ experiments show the complete transformation of schwertmannite to goethite or goethite and hematite (Figs. 4 and 5). Plots of the time-resolved EDXRD data from experiments performed at 80 and 180 °C are shown in Figure 4. Note that in all EDXRD patterns a broad background hump was present throughout the experiments, which was a result of both the spectral intensity profile of the incident beam (Clark et al. 1994) and the scattering from the poorly ordered/amorphous material in the reactor (i.e., schwertmannite,

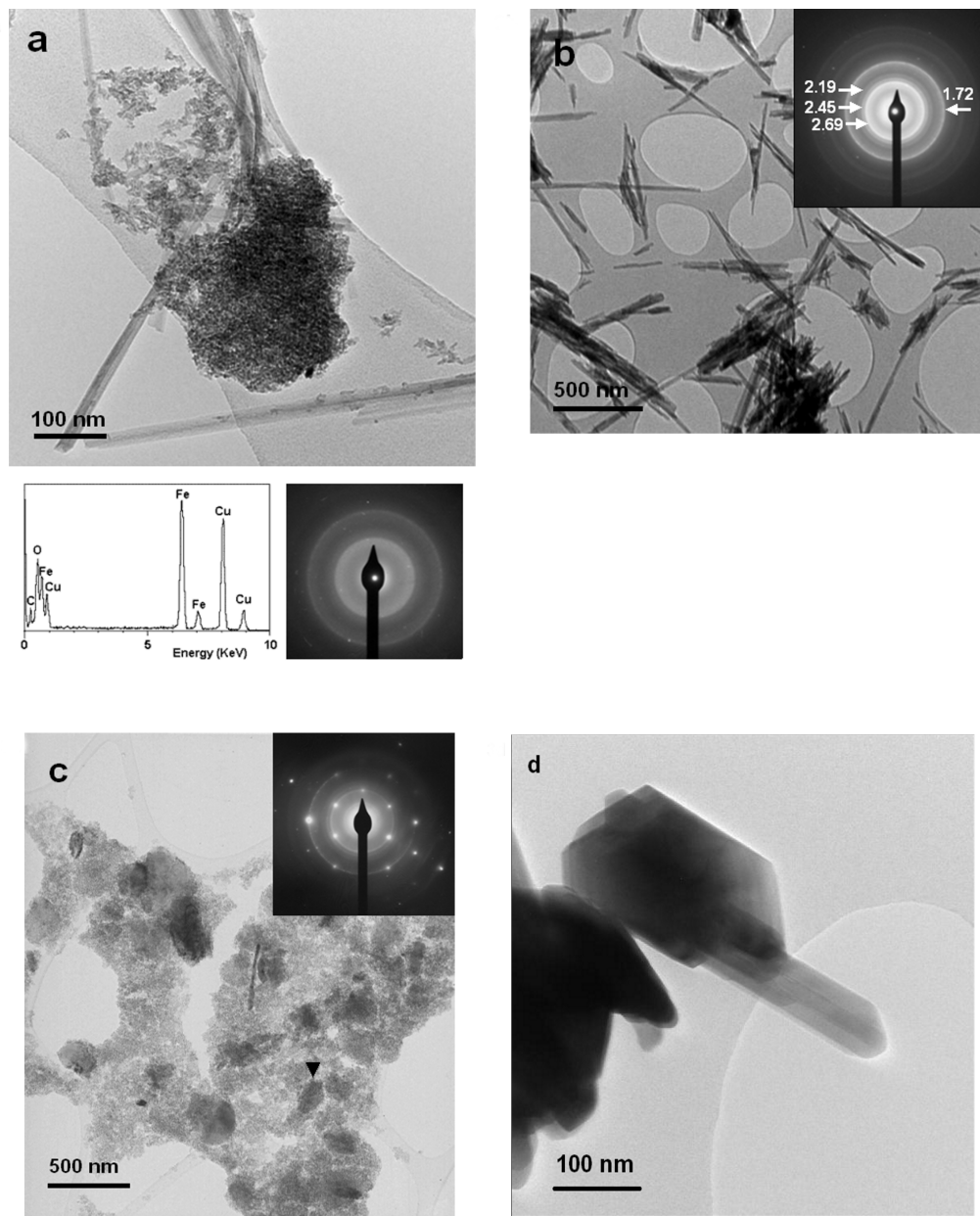


FIGURE 3. TEM images, EDX spectra, and SAED patterns of the solid fractions collected as quenched samples during the reaction at (a) 80 °C and 3000 s, showing a mixture of ferrihydrite and goethite, (b) 80 °C and 24 000 s, showing euhedral goethite laths upon completion of the reaction, (c) 180 °C and 600 s, showing poorly formed hematite crystals in densely aggregated ferrihydrite, and (d) 180 °C and 3000 s, showing goethite laths being overgrown by sub-hexagonal hematite crystals. White arrows indicate *d*-spacings of reflections in angstroms.

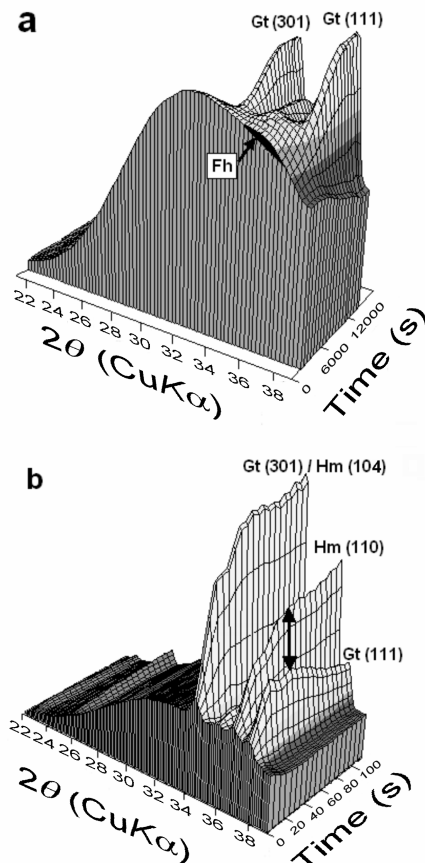


FIGURE 4. Three-dimensional representations of time-resolved EDXRD patterns illustrating the transformation of schwertmannite to (a) goethite at 80 °C and (b) goethite and hematite at 180 °C. Energy was converted to 2θ , using the Bragg equation ($\lambda = 2d\sin\theta$), assuming $\lambda = 1.541 \text{ \AA}$ ($\text{CuK}\alpha$).

ferrihydrate, and NaOH solution). Throughout all the experiments the d -spacings of all the diffraction peaks did not change.

At 60 and 80 °C, an initial broad peak of d -spacing ≈ 2.55 to 2.45 \AA ($2\theta \approx 36^\circ \pm 1$) was observed early in the reaction at times <100 min (Fig. 4a). The phase represented by this peak could not be positively identified in the EDXRD patterns due to its poorly crystalline nature and due to the fact that the data were collected with the solids suspended in solution. However, powder XRD patterns (Fig. 1), TEM micrographs (Figs. 3a and 3c), and SAED (Fig. 3a) of the solid fraction from the early stages of the reaction showed that ferrihydrate formed as an intermediate phase, therefore the observed peak most likely represents the (110) reflection of ferrihydrate. As the reaction progressed this peak became quickly overprinted by the sharper and more intense diffraction peaks of goethite or hematite.

The normalized peak areas of the goethite (111) and the hematite (110) diffraction peaks as a function of time from all the in-situ experiments are plotted in Figure 5. These specific peaks were chosen because of their relatively high intensities and the lack of interference from other peaks. At 60 and 80 °C, after an induction period of ~ 200 and 30 min, respectively, goethite started forming and after ~ 400 and 80 min at 60 and

80 °C, respectively, the goethite growth reached a plateau. At these temperatures, goethite was the sole product of crystallization, which confirmed the results from the off-line experiments presented above (Fig. 1). As the temperature increased the induction period decreased. At $T \geq 90$ °C (Fig. 5), both goethite and hematite were observed to crystallize. TEM micrographs of the particles formed in the early stages (600 s) of the transformation at 180 °C showed densely aggregated and more electron opaque zones within loosely aggregated ferrihydrate. Some of these aggregates contained dense cores that were shown with SAED to be hematite (Fig. 3c). At a later stage of this reaction (3000 s), hematite assumed an irregular platy morphology with poorly formed crystal faces, while goethite formed typical acicular crystals (Figs. 3b and 3d) that ranged in size from a few tens to 1000 nm in length.

With increasing temperature the rate of crystallization of goethite and hematite increased, and hematite became increasingly dominant (Fig. 5). At temperatures ≥ 150 °C, a secondary crystallization stage was observed, in which the goethite to hematite ratio (Gt/Hm; defined as the change in the ratio of the goethite and hematite peak intensities) decreased over time (Fig. 5). TEM characterization of the solid phase produced at 180 °C after 3000 s (i.e., during the secondary crystallization stage) showed that ferrihydrate was no longer present and that the hematite was often observed to overgrow goethite crystals (Fig. 3d). Above 190 °C, the secondary crystallization stage was observed to completion within the time-scale of the experiments (i.e., the complete disappearance of goethite, with hematite as the sole end product). The details of the transformation products and induction times, t_0 , are presented in Table 1.

The pH of the supernatant solutions was buffered by the high concentration of NaOH in the system and remained at an average of 13.2 ($2\sigma = 0.3$) throughout the transformation experiments. The IC analysis (Fig. 6) showed that the majority of the sulfate originally associated with the schwertmannite was released back into solution during the transformation reaction. In Figure 6, the sulfate release is compared with the schwertmannite transformation to goethite plotted in terms of extent of reaction (α). The plot shows that at 80 °C, 84% of the total sulfate in the solid schwertmannite was released by 1200 s, and 96% by 3600 s (Fig. 6a). At 180 °C, 87% of the total sulfate was released by 600 s, and 95% by 1800 s (Fig. 6b).

Based on all the results presented above, the transformation of schwertmannite can be described in three stages: (1) an induction period (t_0), characterized by the absence of resolvable diffraction peaks associated with goethite or hematite and the formation of ferrihydrate; (2) a period of primary crystallization of goethite and/or hematite; and (3) a secondary crystallization stage, in which goethite transforms to hematite. An illustration of how this three stage process occurs is given in Figure 7.

Transformation kinetics and energetics

The time-resolved data for the crystallization of goethite and hematite from schwertmannite (stage 2) were normalized and fitted with the JMAK kinetic model (Fig. 8). For all goethite data at $T \leq 190$ °C, the fitting yielded an average n value of 2.1 ($2\sigma = 0.5$). According to previous studies, the transformation of schwertmannite and ferrihydrate to goethite can be described by a

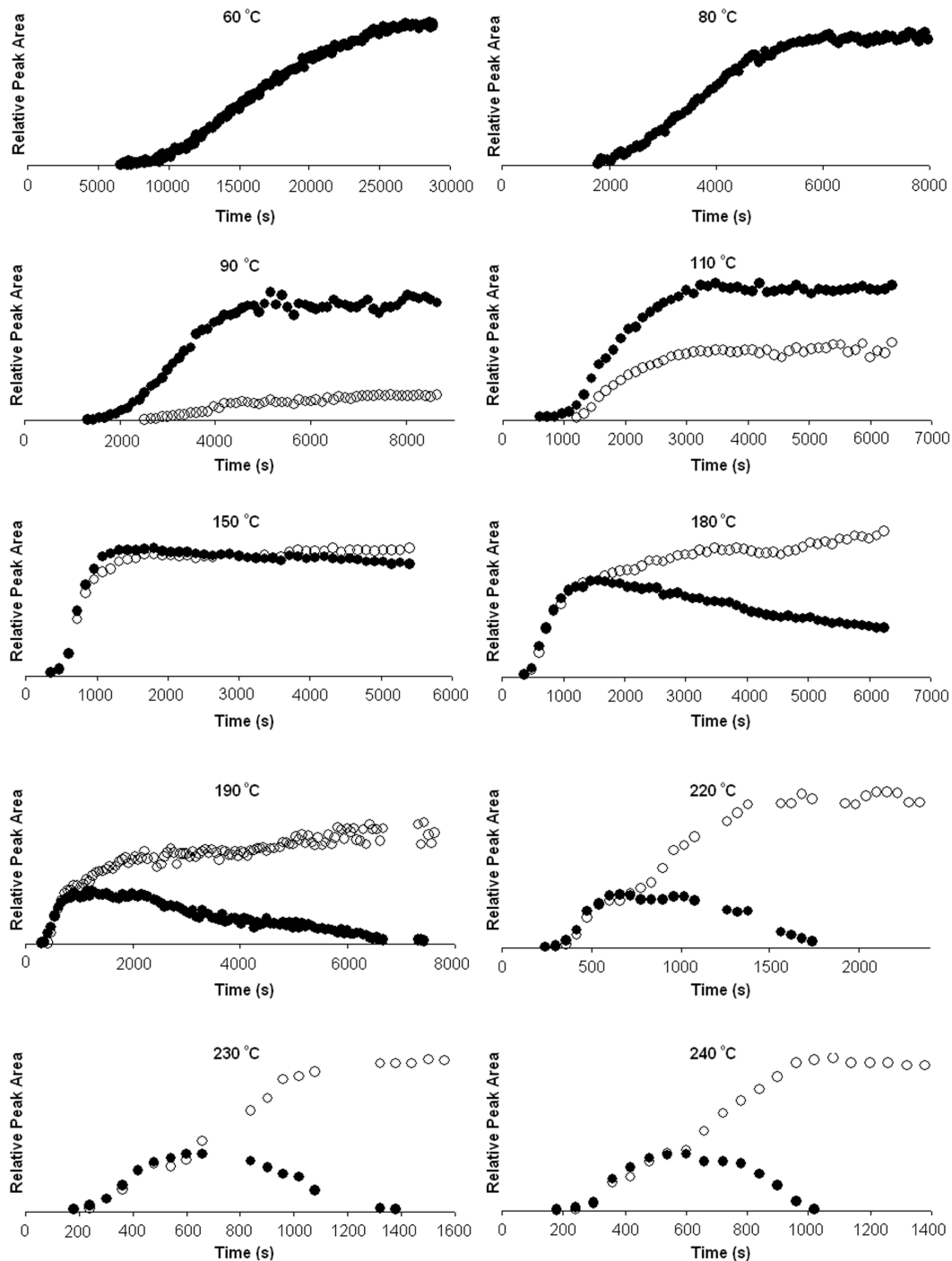


FIGURE 5. Diffraction peak-intensity data displaying the crystallization of goethite (closed circles) and/or hematite (open circles) during the transformation of schwertmannite at temperatures between 60 and 240 °C.

simple first-order reaction ($n = 1$; e.g., Schwertmann and Murad 1983; Schwertmann and Carlson 2005; Shaw et al. 2005). As the n value obtained in this study was considerably larger than 1, and because the transformation mechanism is not expected to change at random across the temperature range, the data were re-fitted with the n value fixed to 2.1. Initial fitting of the hematite formation (stage 2) data to the JMAK model, at temperatures between

90 to 190 °C (Fig. 8b) yielded an average n value of 1.3 ($2\sigma = 0.5$). Previous studies that followed the transformation of ferrihydrite to hematite suggested a first-order reaction equivalent to $n = 1$ (e.g., Fischer and Schwertmann 1975; Schwertmann and Murad 1983; Shaw et al. 2005) and thus the data were re-fitted with n fixed to 1. Data for the secondary crystallization (goethite to hematite) were normalized and fitted to the JMAK

TABLE 1. Details of the induction times for goethite and hematite (t_0) crystallization and the times taken for the completion of both the primary and secondary crystallization periods

T (°C)	Stage 1 (induction period)		Stage 2 (primary crystallization)			Stage 3 (secondary crystallization)	
	Gt t_0 (s)	Hm t_0 (s)	Gt k (s^{-1}), $n = 2.1$	Gt k (s^{-1}), $n = 1$	Hm k (s^{-1}), $n = 1$	Hm t_0 (s)	Hm k (s^{-1}), $n = 1$
60	6515(68)	–	$0.9(0.01) \times 10^{-4}$	$1.9(0.04) \times 10^{-4}$	–	–	–
80	1603(29)	–	$4.2(0.06) \times 10^{-4}$	$9.1(0.3) \times 10^{-4}$	–	–	–
90	1564(60)	2737(57)	$5.4(0.2) \times 10^{-4}$	$10.1(0.8) \times 10^{-4}$	$5.9(0.3) \times 10^{-4}$	–	–
110	633(33)	1241(22)	$9.9(0.2) \times 10^{-4}$	$14.9(0.9) \times 10^{-4}$	$13.5(0.7) \times 10^{-4}$	–	–
150	372(17)	484(10)	$21.9(1.0) \times 10^{-4}$	$44.9(7.4) \times 10^{-4}$	$29.1(0.7) \times 10^{-4}$	–	–
180	340(14)	467(8)	$29.4(0.6) \times 10^{-4}$	$59.0(3.9) \times 10^{-4}$	$33.5(1.5) \times 10^{-4}$	–	–
190	327(17)	428(8)	$40.8(0.2) \times 10^{-4}$	$69.2(4.9) \times 10^{-4}$	$60.7(5.0) \times 10^{-4}$	1020	$4.5(0.2) \times 10^{-4}$
220	–	–	–	–	–	660	$28.7(1.8) \times 10^{-4}$
230	–	–	–	–	–	600	$42.3(3.6) \times 10^{-4}$
240	–	–	–	–	–	600	$51.7(4.0) \times 10^{-4}$
$E_{a(nucl)}$			26(1)	27(1)	25(1)		
$E_{a(cryst)}$			33(1)	30(1)	28(1)		103(3)

Notes: The conditional rate constants, k , were calculated by fitting the time resolved and normalized data from the transformation of schwertmannite to goethite and hematite to the JMAK model, with n fixed to 2.1 and 1 for goethite, and 1 for hematite. The k values for the transformation of goethite to hematite, with n fixed to 1, are also displayed. The activation energies of nucleation, $E_{a(nucl)}$ and crystallization, $E_{a(cryst)}$ are also shown.

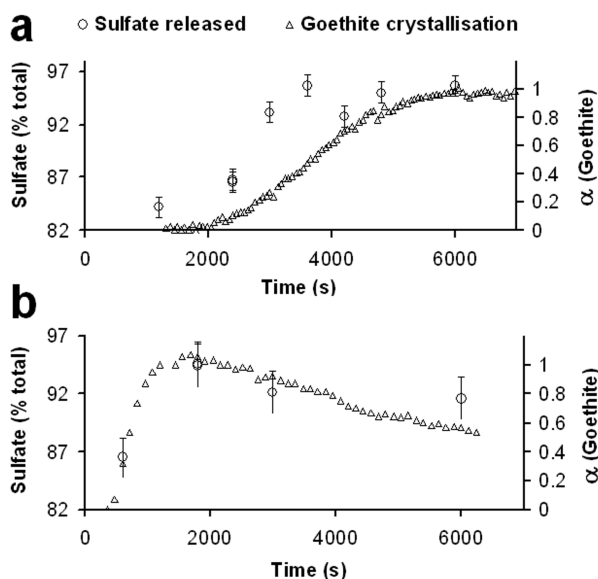


FIGURE 6. Sulfate concentration in supernatant (as a percentage of the total sulfate in the system) during the transformation of schwertmannite at (a) 80 °C and (b) 180 °C. Note that some measurements were performed twice to monitor the data quality. The time-resolved data for the crystallization of goethite in terms of α are also displayed for comparison.

model (Fig. 9), where t_0 was chosen as the time corresponding to the apex of the goethite growth curve (see Fig. 7). The data generally fit the model well, though stirring problems caused scatter in the data for the 190 °C experiment. Fitting the data with n as a free parameter resulted in an average n value of 1.3 ($2\sigma = 0.4$). No data on the reaction order of this transformation reaction was available from the literature and thus the data were re-fitted using $n = 1$.

The activation energies of nucleation [$E_{a(nucl)}$] and crystallization [$E_{a(cryst)}$] for the primary and secondary goethite and/or hematite formation were calculated using the Arrhenius equations (Table 1). Above 190 °C, the faster crystallization rates lead to a lower number of diffraction patterns describing the growth process and hence fewer data points to which the kinetic model could be fitted. This caused a significant increase in the errors in k , t_0 , and n , and consequently these results were omitted from the

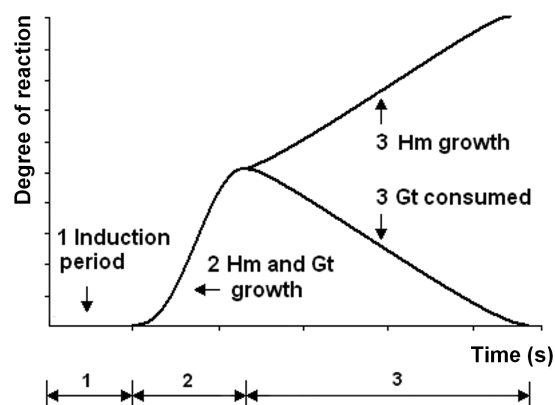


FIGURE 7. Schematic diagram illustrating the three stages of transformation from schwertmannite to goethite and hematite.

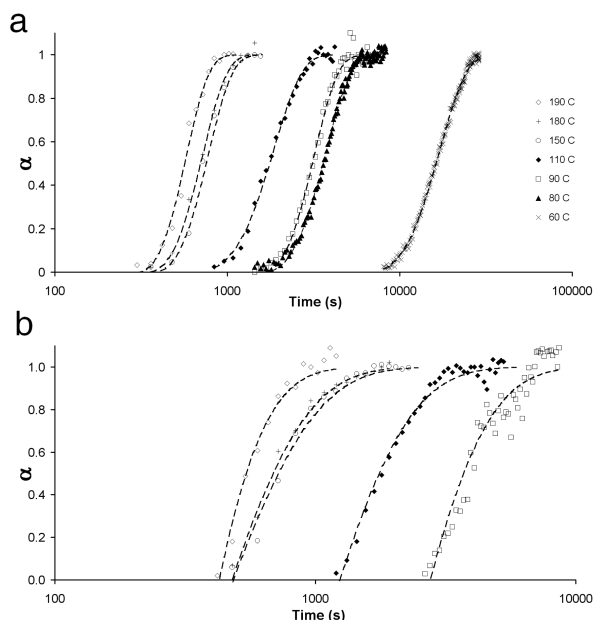


FIGURE 8. Degree of reaction (α) of (a) goethite and (b) hematite formation as a function of time during the transformation of schwertmannite. The dashed lines are fits of the JMAK kinetic model to each data set.

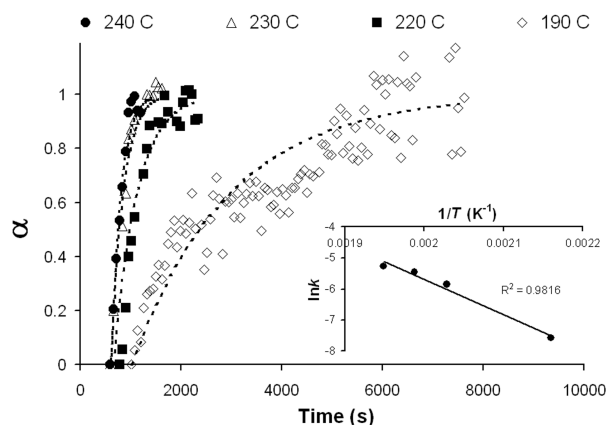


FIGURE 9. Degree of reaction (α) showing the formation of hematite from goethite, for temperatures between 190 to 240 °C, fitted to the JMAK kinetic model, with $n = 1$. Inset shows the Arrhenius plot of the k values.

calculations of the activation energies. The linearity of the data in the Arrhenius plots (Figs. 9 and 10) indicates that the mechanisms were constant across all experimental conditions.

DISCUSSION

Schwertmannite starting material

The morphology of the particles within the starting material was typical of both synthetic and naturally occurring schwertmannite described in previous studies (Bigham et al. 1990, 1994; Bigham and Nordstrom 2000; Carlson et al. 2002; Regenspurg et al. 2004; Loan et al. 2004). The sulfate content of the schwertmannite was at the high end of the range reported by Bigham et al. (1990) for both synthetic (0.1 to 15.5 wt%) and natural (8.5 to 14.1%) samples. This is likely to be due to the precipitation of the schwertmannite from solutions with a high initial sulfate concentration. The total iron content (42.0 ± 0.4 wt%) falls between the ranges for synthetic (43.2 to 56.7 wt%) and natural (39.4 to 41.8 wt%) schwertmannite as reported by Bigham et al. (1990). The mode of precipitation applied in this study produced a starting material that was chemically and morphologically typical of both natural and synthetic schwertmannite and was, therefore, a good basis for studies replicating environmentally related processes.

Primary crystallization: Goethite and hematite formation

Goethite formation. At temperatures ≤ 80 °C goethite was the only observed stable end-product. This is in agreement with previous studies on the transformation of natural and synthetic schwertmannite at 20–25 °C and pH 1.9–9, which showed a partial or complete transformation of schwertmannite to goethite. TEM and XRD analyses demonstrated that schwertmannite transforms to goethite via a ferrihydrite intermediate. The crystallization data from this study, therefore, can be compared with results from previous studies characterizing the transformation of ferrihydrite to goethite under similar chemical conditions.

Mackay (1960) and later Schwertmann and Murad (1983) demonstrated that the transformation of ferrihydrite to goethite under aqueous conditions occurs via a reconstructive dissolution/

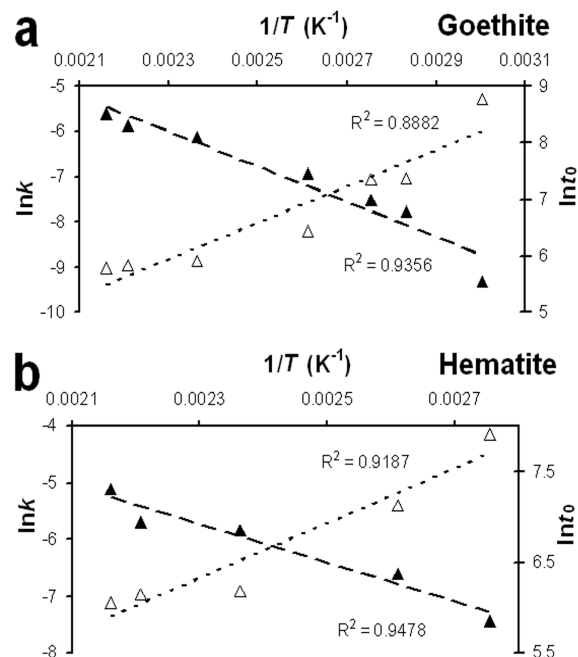


FIGURE 10. Arrhenius plots of data from the induction times (t_0 ; open triangles) and growth rates (k ; closed triangles) for the transformation of schwertmannite to (a) goethite and (b) hematite.

re-precipitation mechanism and follows pseudo-first-order kinetics. This mechanism is consistent with the observed transformation to goethite under alkaline conditions where iron solubility is high. Time-resolved EDXRD studies of goethite crystallization from ferrihydrite at pH 13.7 revealed that goethite nucleates directly from solution (i.e., homogenous nucleation) and crystal growth occurs via a surface-controlled mechanism (Shaw et al. 2005). Also, fitting the goethite EDXRD peak growth to the JMAK kinetic model yielded an exponent of $n = 1$, which is equivalent to pseudo-first-order kinetics. However, fitting the peak area growth data for goethite formation from the current study yielded $n = 2.1$ (Fig. 8a) suggesting that additional factors influenced the crystallization of schwertmannite to goethite. This difference in the exponents is likely to reflect the effect of sulfate from the schwertmannite on some part of the goethite formation process. Previous studies have shown that oxyanions (e.g., sulfate) usually adsorb to ferrihydrite as binuclear, inner-sphere surface complexes and can impede mineral dissolution because the simultaneous removal of two or more metal centers is energetically unfavorable (Parfitt and Smart 1978). For example, Biber et al. (1994) showed that oxyanions (e.g., phosphate) act as strong inhibitors in the dissolution of iron (oxy)hydroxides. These results are supported by the findings of Lin et al. (2003), who studied the transformation of Cd-doped ferrihydrite in the presence of sulfate, nitrate, and chloride. They showed that the rate of transformation was significantly lower for the sulfate-rich system and postulated that a strong ferrihydrite-sulfate interaction may immobilize the ferrihydrite surface and suppress dissolution. Given the evidence from these previous studies, we suggest that the inhibition of ferrihydrite dissolution by sorbed sulfate

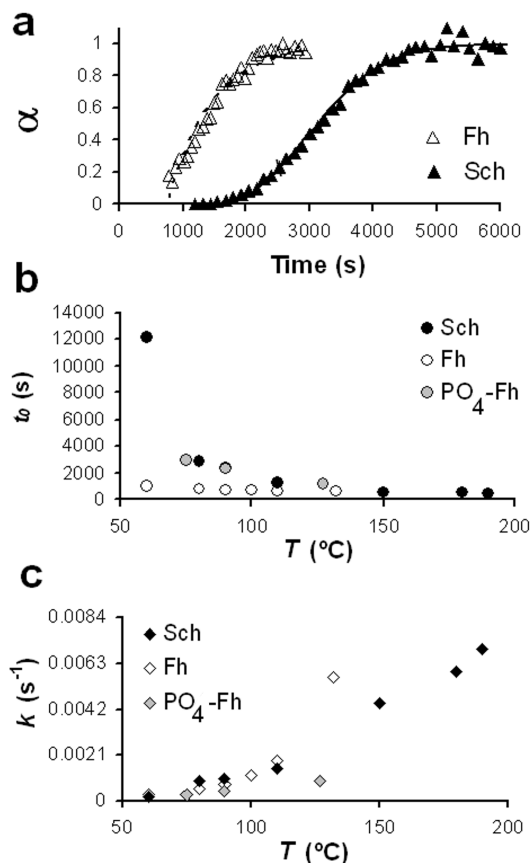


FIGURE 11. Time or temperature dependent plots comparing data for the crystallization of goethite from schwertmannite (this study), with data from goethite formation from pure ferrihydrite (Fh) or PO_4 -doped ferrihydrite (PO_4 -Fh) from Shaw et al, 2005. (a) Degree of reaction (α) at 90 °C; (b) induction periods (t_0); and (c) the conditional rate constants (k) as a function of temperature.

had a significant effect on goethite formation. The retardation of ferrihydrite dissolution limits the supply of ferric iron being released into solution and thus retards goethite crystal growth and/or nucleation rates. Further information about this process was obtained by comparing data from the current study with the in situ, time-resolved, EDXRD data on the transformation of pure-ferrihydrite and phosphate-doped ferrihydrite to goethite in pH 13.7 from Shaw et al. (2005).

The induction times for goethite growth from schwertmannite were longer than those reported for goethite formation from pure ferrihydrite and similar to those for phosphate-doped ferrihydrite (Figs. 11a and 11b). This was despite the large differences in initial dopant concentrations (3% PO_4/Fe vs. 35% SO_4/Fe), which reflects the fact that phosphate has a higher affinity for the ferric (oxy)hydroxide octahedra than sulfate (e.g., Liu et al. 1999). Phosphate has been shown to inhibit ferrihydrite dissolution so strongly that homogenous nucleation of goethite is blocked, thus forcing heterogeneous nucleation of goethite on hematite (Bárron et al. 1997; Shaw et al. 2005). No evidence for this nucleation mechanism was observed in the transformation of schwertmannite. The longer induction times for the

crystallization of schwertmannite to goethite compared to the pure ferrihydrite system, however, imply that the reduced rate of ferrihydrite dissolution caused by sorbed sulfate does inhibit the rate of goethite nucleation.

Comparison of the goethite EDXRD peak growth profiles from pure ferrihydrite and schwertmannite show a clear difference in the growth kinetics (Fig. 11a). Qualitatively, the rate of goethite crystallization during the early stages of the reaction was significantly slower for schwertmannite than for pure ferrihydrite. This indicates that, during the early stages of growth, sulfate inhibited the formation of goethite. This could occur via two possible mechanisms. First, the slow release of ferric iron due to sulfate sorbed to the ferrihydrite (e.g., coprecipitated within the ferrihydrite structure or within isolated nanopores in particle aggregates) could limit the growth of the goethite particles. Second, sulfate could adsorb to the surface of the growing goethite particles and thus block growth sites on the crystals. There is a very little sulfate associated with the final crystalline goethite (Fig. 6a), which is due to the high pH of the solution where sulfate adsorption is very low. This suggests the first mechanism is most likely, because the sulfate will not adsorb to the growing goethite crystals under high pH conditions. To quantitatively compare the crystallization rates obtained in this study to those of Shaw et al. (2005), the goethite growth data from this study were re-fitted using an n value of 1 (instead of 2.1). This was achieved by omitting data where $\alpha < 0.1$ –0.2 from the fitting such that the data that deviated from a pseudo-first-order model were discounted. The comparison between the values of k from this study and those from Shaw et al. (2005) are plotted in Figure 11c. The rates for the transformation of schwertmannite were slightly lower than those for transformation of pure ferrihydrite, but the crystallization rate for the phosphate-doped system were significantly lower than for either the pure or sulfate-doped system. Again, this indicates that the presence of sulfate inhibits goethite formation, but to a much lesser extent than phosphate. Measurement of the sulfate concentration in the supernatant (Fig. 6a) showed that a fraction of the total sulfate ($13 \pm 1\%$) remained associated with the ferrihydrite intermediate (e.g., first 40 min). However, as the reaction progressed, the sulfate continued to be released into solution and at the end of the transformation the final goethite was almost sulfate-free. This implies that the sulfate is mostly associated with the ferrihydrite and does not become associated with the crystalline goethite. This indicates that the slower crystallization rates at the early stages of goethite formation were due to the slow dissolution of the sulfate-doped ferrihydrite, as opposed to the blocking of goethite growth by sorbed sulfate. Also, it seems sulfate does reduce the growth rate of goethite relative to the pure ferrihydrite system, but to a much lesser extent than phosphate, which is further evidence that the effect of sorbed sulfate on the growing goethite crystals is small.

For the transformation of pure ferrihydrite to goethite, Shaw et al. (2005) calculated an $E_{a(\text{nuc})} = 7 \pm 1$ kJ/mol, which is indicative of simple homogeneous nucleation from solution with the diffusion of ions through the aqueous solution being the controlling mechanism. The $E_{a(\text{nuc})}$ determined for goethite crystallization in this study was significantly larger, at 27 ± 1 kJ/mol, and exceeded the upper limit (i.e., 21 kJ/mol) for aqueous

diffusion controlled reactions (Lasaga 1998). The increase in $E_{a(\text{nucl})}$ relative to the pure ferrihydrite system further supports the hypothesis that sulfate inhibits the nucleation of goethite, which is caused by a reduction in the rate of ferrihydrite dissolution due to adsorbed sulfate. The $E_{a(\text{cryst})}$ (33 ± 1 kJ/mol) lies within error of the minimum value of the range given for a surface controlled reaction (33.5 kJ/mol; Lasaga 1998). The well-defined crystal faces of the goethite crystals as seen in TEM images (Fig. 3b) also support a surface controlled mechanism (Lasaga 1998). The $E_{a(\text{cryst})}$ is comparable to the value obtained for goethite growing from pure ferrihydrite (39 ± 3 kJ/mol, Shaw et al. 2005) indicating that although sulfate has the effect of decreasing the rate of goethite crystallization, at least during the early stages, the overall energetics of the reaction mechanism is unchanged. This further supports the hypothesis that sulfate has little direct interaction with the growing goethite crystal, but limits the supply of ferric iron due its effect on the dissolution of ferrihydrite.

Hematite formation. With increasing temperature (≥ 90 °C) the Hm/Gt ratio increased and at ≥ 150 °C, goethite was observed to be a fully intermediate phase on the time scale of the experiments. TEM images of the early stages of the transformation of schwertmannite at 180 °C (Fig. 3c) suggest that hematite formed via aggregation of ferrihydrite nanoparticles. The transformation of ferrihydrite to hematite is thought to proceed via an aggregation of the ferrihydrite followed by a crystallization process within the aggregates (Schwertmann 1959; Schwertmann and Fischer 1966; Towe and Bradley 1967; Fischer 1971; Fischer and Schwertmann 1975; Christensen et al. 1980; Schwertmann and Murad 1983). The presence of water is essential in this process with isotopic studies suggesting that the crystallization occurs via short-range dissolution and reprecipitation within the aggregates (Bao and Koch 1999). This mechanism is consistent with hematite formation at pH values close to the PZC of ferrihydrite (pH 7.8), where aggregation occurs readily and ferric iron solubility is low. Hematite was not expected to form at the high pH conditions in the current study (pH 13.2). Indeed, Jönsson et al. (2005) reported goethite to be the sole end product of schwertmannite transformation at pH 9 at room temperature after 17 months. It is likely that hematite was stabilized by the high-temperature conditions of the present study, which promoted the transformation of ferrihydrite to hematite relative to goethite. Similar observations have been reported in studies on the transformation of ferrihydrite to hematite in the pH range 3 to 9 at elevated temperatures (e.g., Schwertmann and Fischer 1966; Fischer and Schwertmann 1975; Gálvez et al. 1999). However, Shaw et al. (2005) followed the transformation of ferrihydrite in 1 M KOH and found goethite to be the only reaction product at temperatures of up to 137 °C, while in the current study, hematite was observed at temperatures as low as 90 °C. This suggests that the association of sulfate with the ferrihydrite intermediate favored the mechanism of hematite formation and/or inhibited the mechanism of goethite formation. This is in agreement with the findings of Lin et al. (2003), who showed that the Hm/Gt ratio increased upon transformation of Cd-doped ferrihydrite in the presence of sulfate, when compared to the transformation in the presence of nitrate or chloride. They suggested that sulfate stabilized the ferrihydrite surface and thus hindered ferrihydrite dissolution. We propose that a similar mechanism can account

for the crystallization of hematite from schwertmannite and that the presence of sulfate favored the formation of hematite over goethite because it inhibited ferrihydrite dissolution and thereby promoted the transformation to hematite.

The growth profiles for hematite formation showed a near first-order response at temperatures ≤ 190 °C (Fig. 8b). This is in agreement with previous studies that have reported the conversion of ferrihydrite to hematite follows a first-order dependence with respect to ferrihydrite (e.g., Fischer and Schwertmann 1975; Schwertmann and Murad 1983; Shaw et al. 2005). This indicates that, unlike goethite formation, sulfate was not observed to alter the mechanism of hematite formation. The value for $E_{a(\text{nucl})}$ for hematite formation derived in this study (25 ± 1 kJ/mol), is within error of previously published activation energies (Shaw et al. 2005), which suggests that sulfate has little effect on the aggregation of ferrihydrite, which precedes hematite crystallization. The $E_{a(\text{cryst})}$ determined for hematite (28 ± 1 kJ/mol) is significantly lower than that reported for hematite crystallized from pure ferrihydrite at pH 10.7 (69 ± 6 kJ/mol; Shaw et al. 2005). We suggest that the lower activation energy is related to the high pH of formation where the solubility of ferric iron is high. The higher concentration of dissolved iron within the nano-pores of the aggregated particles aids the diffusion of the ions and therefore lowers the activation energy.

Secondary transformation of goethite to hematite

TEM characterization of the quenched products from the secondary crystallization stage illustrates the association between goethite and hematite crystals and the absence of ferrihydrite (Fig. 3d). This evidence, along with the observed increase in the relative peak area of hematite at the expense of goethite from the EDXRD data (Fig. 5), suggests that this second transformation is a direct transformation of goethite to hematite. Goss (1987) reported a diffusive control on the dry transformation of goethite to hematite, which is consistent with the migration of hydroxyls and protons from the structure. Therefore, it is possible that a simple diffusion-controlled mechanism can describe the transformation of goethite to hematite in solution. However, studies involving the non-isothermal dry heating of goethite and its transformation to hematite showed that the dehydration reaction occurs at temperature >200 °C (Fan et al. 2006). The transformation of goethite to hematite in this study was observed to occur at lower temperatures (150 °C), and therefore it is likely that water facilitates the reaction.

In fitting the hematite growth data to the JMAK kinetic model, n was fixed to 1, which is consistent with a diffusion-controlled, 2-D growth (Hulbert 1969) that would be predicted by a direct dehydration/transformation mechanism. This produced a good fit to all the data and yielded an $E_{a(\text{cryst})} = 103 \pm 3$ kJ/mol. However, Fan et al. (2006) found that a 3-D growth mechanism best described the dry thermal transformation of goethite to hematite. This mechanism would yield $n = 1.5$ (Hulbert 1969). Re-fitting the data using $n = 1.5$ (data not shown) yielded $E_{a(\text{cryst})} = 99 \pm 3$ kJ/mol, which is within the error margin of the value calculated for $n = 1$ (Table 1). Therefore the dimensionality of growth used in the kinetic model has a negligible effect on the calculated activation energy. The derived value for the $E_{a(\text{cryst})}$ for hematite from goethite (103 ± 3 kJ/mol) falls within the range

of values reported for this dehydroxylation reaction (88 to 247 kJ/mol; Cornell and Schwertmann 2003), but is also within the accepted range for diffusion and surface controlled crystallization reactions (Lasaga 1998).

The structures of hematite and goethite have a similar anion framework, with 3 unit cells of goethite stacked along the *c* axis forming 1 unit cell of hematite. Within this common anion framework the *c* axis of goethite and hematite are parallel. This relationship was observed in TEM micrographs (Fig. 3d, where the *c* axes of both phases correspond to the viewing axis). A direct topotactic transformation would involve dehydration and the rearrangement of the cations (Cornell and Schwertmann 2003; Cudennec and Lecerf 2005). Studies of goethite dehydration in air indicate that the transformation occurs between 260 and 320 °C, so it seems unlikely that the direct transformation would occur at lower temperatures and in the presence of water. We propose that the transformation of goethite to hematite must be facilitated by the presence of water in the system, but some topotactic relationship between the two phases is retained during the reaction. The exact mechanism by which water facilitates this process is not clear, but may involve dissolution of goethite and reprecipitation of hematite within the particle aggregates.

IMPLICATIONS AND CONCLUDING REMARKS

We proposed a new system for the transformation of schwertmannite to goethite and/or hematite with the various pathways illustrated in Figure 12. The kinetic and energetic information provide strong evidence for a dissolution/re-precipitation mechanism for the formation of goethite from schwertmannite, with the presence of sulfate significantly retarding the dissolution of the ferrihydrite intermediate. This impedes the early stages of goethite nucleation and growth relative to the formation of goethite from pure ferrihydrite. Our data have also shown that sulfate inhibits the dissolution of the ferrihydrite intermediate and therefore favors the formation of hematite relative to goethite.

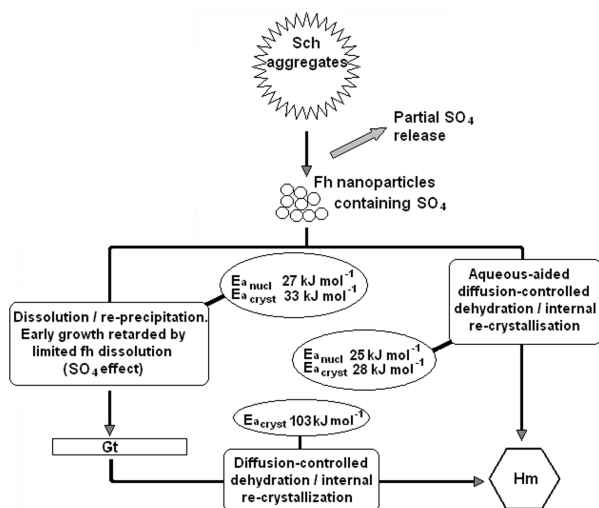


FIGURE 12. Schematic outlining the reaction steps in the transformation of schwertmannite to goethite and/or hematite. The derived mechanisms and activation energies are shown for each reaction.

This study has shown that sulfate is released into solution during the transformation process. Within AMD environments, other toxic oxyanions (e.g., arsenate and chromate) can be abundant within associated surface- and groundwaters. Many of these oxyanions have been shown to substitute for sulfate within the schwertmannite structure and therefore could be released during crystallization to goethite and/or hematite. The crystallization process is likely to be slow within AMD environments, due to low temperature and neutral-acid pH regimes, and the potential release of contaminants during crystallization, therefore, could occur many years after the oxyanions were sequestered by schwertmannite. The transformation process could have significant implications for predicting the long term release of contaminants within AMD sites and for any remediation and stabilization strategies employed.

ACKNOWLEDGMENTS

This study was funded by a Natural Environmental Research Council research studentship (NER/SA/2003/11273) with a CASE award from Diamond Ltd. Access to the Synchrotron Radiation Source, Daresbury Laboratory, was funded by two CCLRC access grants awarded to SS. The authors thank Dave Taylor, station scientist on station 16.4, for his assistance and Andy Brown from the Leeds Electron Microscopy facilities in the Institute of Materials for his assistance with TEM work.

REFERENCES CITED

- Avrami, M. (1939) Kinetics of phase change, I. *Journal of Chemical Physics*, 7, 1103–1112.
- (1940) Kinetics of phase change, II. *Journal of Chemical Physics*, 8, 212–224.
- Bao, H. and Koch, P.L. (1999) Oxygen isotope fractionation in ferric oxide-water systems: low temperature synthesis. *Geochimica et Cosmochimica Acta*, 63, 599–613.
- Barham, R.J. (1997) Schwertmannite: A unique mineral, contains a replaceable ligand, transforms to jarosites, hematites, and/or basic iron sulfate. *Journal of Materials Research*, 12, 2751–2758.
- Bárron, V., Galvez, N., Hochella, M.F., Jr., and Torrent, J. (1997) Epitaxial overgrowth of goethite on hematite synthesized in phosphate media: A scanning force and transmission electron microscopy study. *American Mineralogist*, 82, 1091–1100.
- Biber, M.V., dos Santos Afonso, M., and Stumm, W. (1994) The coordination chemistry of weathering: IV. Inhibition of the dissolution of oxide minerals. *Geochimica et Cosmochimica Acta*, 58, 1999–2010.
- Bigham, J.M. and Nordstrom, D.K. (2000) Iron and aluminum hydroxysulfates from acid sulfate waters. In C.N. Alpers, J.L. Jambor, and D.K. Nordstrom, Eds., *Sulfate Minerals—Crystallography, Geochemistry and Environmental Significance*, 40, p. 351–403. *Reviews in Mineralogy and Geochemistry*, Mineralogical Society of America, Chantilly, Virginia.
- Bigham, J.M., Schwertmann, U., Carlson, L., and Murad, E. (1990) A poorly crystallized oxyhydroxysulfate of iron formed by bacterial oxidation of Fe(II) in acid mine waters. *Geochimica et Cosmochimica Acta*, 54, 2743–2758.
- Bigham, J.M., Carlson, L., and Murad, E. (1994) Schwertmannite, a new iron oxyhydroxysulfate from Pyhäsalmi, Finland, and other localities. *Mineralogical Magazine*, 58, 641–648.
- Bigham, J.M., Schwertmann, U., Traina, S.J., Winland, R.L., and Wolf, M. (1996) Schwertmannite and the chemical modeling of iron in acid sulfate waters. *Geochimica et Cosmochimica Acta*, 60, 2111–2121.
- Brown, J.B. (1971) Jarosite-goethite stabilities at 25 °C, 1 Atm. *Mineralium Deposita*, 6, 245–252.
- Carlson, L., Bigham, J.K., Schwertmann, U., Kyek, A., and Wagner, F. (2002) Scavenging of As from acid mine drainage by schwertmannite and ferrihydrite: A comparison with synthetic analogues. *Environmental Science and Technology*, 36, 1712–1719.
- Chery, R.W. and Coelho, A. (1992) A fundamental parameters approach to X-ray line-profile fitting. *Journal of Applied Crystallography*, 25, 109–121.
- Childs, C.W., Inoue, K., and Mizota, C. (1998) Natural and anthropogenic schwertmannites from Towada-Hachimantai National Park, Honshu, Japan. *Chemical Geology*, 144, 81–86.
- Christensen, A.N., Convert, P., and Lehmann, M.S. (1980) Hydrothermal crystal-growth rate of goethite and hematite from amorphous iron(III) hydroxide investigated by X-ray-diffraction and neutron-diffraction. *Acta Chemica Scandinavica Series A: Physical and Inorganic Chemistry*, 34, 771–776.

- Clark, S.M., Irvin, P., Flaherty, J., Rathbone, T., Wong, H.V., Evans, J.S.O., and O'Hare, D. (1994) Apparatus for the in situ kinetic study of reactions involving air sensitive materials using energy-dispersive powder diffraction. *Review of Scientific Instruments*, 65, 2210–2213.
- Cornell, R.M. and Schwertmann, U. (2003) *The iron oxides: Structure, properties, reactions, occurrences and uses*, 664 p. VCH Verlag, Weinheim.
- Cravotta, C.A.I., Brady, K.B.C., Rose, A.W., and Douds, J.B. (1999) Frequency distribution of the pH of coal-mine drainage in Pennsylvania DW. U.S. Geological Survey Toxic Substances Hydrology Program-Proc Technical Meeting. U.S. Geological Survey Water-Research Investigation Report, 99-4018A, p. 313–324.
- Cudennec, Y. and Lecerf, A. (2005) Topotactic transformations of goethite and lepidocrocite into hematite and maghemite. *Solid State Sciences* 7, 520–529.
- Fan, H.L., Song, B.Z., and Li, Q.X. (2006) Thermal behavior of goethite during transformation to hematite. *Materials Chemistry and Physics*, 98, 148–153.
- Finger, L.W. (1989) Synchrotron powder diffraction. In D.L. Bish and J.E. Post, Eds., *Modern powder diffraction*, 20, p. 309–330. Reviews in Mineralogy, Mineralogical Society of America, Chantilly, Virginia.
- Fischer, W.R. (1971) Modellversuch zur Bildung und Auflösung von Goethit und amorphen Eisenoxiden im Boden. Dissertation, Technischen Universität, München.
- Fischer, W.R. and Schwertmann, U. (1975) The formation of hematite from amorphous iron(III) hydroxide. *Clays and Clay Minerals*, 23, 33–37.
- Fukushi, K., Sato, T., and Yanase, N. (2003a) Solid solution reactions in As(V) sorption by schwertmannite. *Environmental Science and Technology*, 37, 3581–3586.
- Fukushi, K., Sasaki, M., Sato, T., Yanase, N., Amano, H., and Ikeda, H. (2003b) A natural attenuation of arsenic in drainage from an abandoned arsenic mine dump. *Applied Geochemistry*, 18, 1267–1278.
- Fukushi, K., Sato, T., Yanase, N., Minato, J., and Yamada, H. (2004) Arsenate sorption on schwertmannite. *American Mineralogist*, 89, 1728–1734.
- Gagliano, W.B., Brill, M.R., Bigham, J.M., Jones, F.S., and Traina, S.J. (2004) Chemistry and mineralogy of ochreous sediments in a constructed mine drainage wetland. *Geochimica et Cosmochimica Acta*, 68, 2119–2128.
- Gálvez, N., Barrón, V., and Torrent, J. (1999) Effect of phosphate on the crystallization of hematite, goethite, and lepidocrocite from ferrihydrite. *Clays and Clay Minerals*, 47, 304–311.
- Goss, C.J. (1987) The kinetics and reaction-mechanism of the goethite to hematite transformation. *Mineralogical Magazine*, 51, 437–451.
- Hulbert, S.F. (1969) Models of solid-state reactions in powder compacts: A review. *Journal of the British Ceramics Society*, 6, 11–20.
- Jambor, J.L. and Dutrizac, J.E. (1998) Occurrence and constitution of natural and synthetic ferrihydrite, a widespread iron oxyhydroxide. *Chemical Reviews*, 98, 2549–2585.
- Janney, D.E., Cowley, J.M., and Buseck, P.R. (2001) Structure of synthetic 6-line ferrihydrite by electron nanodiffraction. *American Mineralogist*, 86, 327–335.
- Jiang, W.T. and Chen, C.J. (2005) Formation and transformation of schwertmannite in acid-mine-drainage deposits of the Chinkuashih mining area, northern Taiwan. *Geochimica et Cosmochimica Acta*, 69, A774–A774.
- Johnson, P.F. and Mehl, R.F. (1939) Reaction kinetics in processes of nucleation and growth. American Institute of Mining Engineering, Technical Publication, 1089, 1–27.
- Jönsson, J., Persson, P., Sjöberg, S., and Lövgren, L. (2005) Schwertmannite precipitated from acid mine drainage: Phase transformation, sulfate release, and surface properties. *Applied Geochemistry*, 20, 179–191.
- Kaschiev, D. (1969) Solution of the non-steady state problem in nucleation kinetics. *Surface Science*, 14, 209–220.
- Lasaga, A.C. (1998) *Kinetic Theory in the Earth Sciences*, 811 p. Princeton University Press, New Jersey.
- Lin, X., Burns, R.C., and Lawrance, G.A. (2003) Effect of cadmium(II) and anion type on the aging of ferrihydrite and its subsequent leaching under neutral and alkaline conditions. *Water, Air, and Soil Pollution*, 143, 155–177.
- Liu, F., He, J., Colombo, C., and Violante, A. (1999) Competitive adsorption of sulfate and oxalate on goethite in the absence or presence of phosphate. *Soil Science*, 164, 180–189.
- Loan, M., Cowley, J.M., Hart, R., and Parkinson, G.M. (2004) Evidence on the structure of synthetic schwertmannite. *American Mineralogist*, 89, 1735–1742.
- Mackay, A.L. (1960) Structural transformations in the iron oxide-hydroxide system. *Acta Crystallographica*, 13, 1095–1095.
- Parfitt, R.L. and Smart, R.S.C. (1978) The mechanism of sulfate adsorption on iron oxides. *Soil Science Society of America Journal*, 42, 48–50.
- Regenspurg, S. and Peiffer, S. (2005) Arsenate and chromate incorporation in schwertmannite. *Applied Geochemistry*, 20, 1226–1239.
- Regenspurg, S., Brand, A., and Peiffer, S. (2004) Formation and stability of schwertmannite in acidic mining lakes. *Geochimica et Cosmochimica Acta*, 68, 1185–1197.
- Schroth, A.W. and Parnell, R.A., Jr. (2005) Trace metal retention through the schwertmannite to goethite transformation as observed in a field Alta Mine, Montana. *Applied Geochemistry*, 20, 907–917.
- Schwertmann, U. (1959) Die fraktionierte Extraktion der freien Eisenoxide in Böden, ihre mineralogischen Formen und ihre Entstehungsweisen. *Zeitschrift für Pflanzenernährung, Düngung und Bodenkunde*, 105, 194–202.
- Schwertmann, U. and Carlson, L. (2005) The pH-dependent transformation of schwertmannite to goethite at 25 °C. *Clay Minerals* 40, 63–66.
- Schwertmann, U. and Fischer, W. (1966) Zur bildung von α -FeOOH und α -Fe₂O₃ aus amorphem Eisen(III) hydroxid. *Zeitschrift Für Anorganische Und Allgemeine Chemie*, 346, 137–142.
- Schwertmann, U. and Murad, E. (1983) Effect of pH on the formation of goethite and hematite from ferrihydrite. *Clays and Clay Minerals*, 31, 277–284.
- Shaw, S., Clark, S.M., and Henderson, C.M.B. (2000) Hydrothermal formation of the calcium silicate hydrates, tobermorite [Ca₅Si₆O₁₆(OH)₂·4H₂O] and xonolite [Ca₆Si₆O₁₇(OH)₂]: an in situ synchrotron study. *Chemical Geology*, 167, 129–140.
- Shaw, S., Pepper, S.H., Bryan, N.D., and Livens, F.R. (2005) The kinetics and mechanisms of goethite and hematite crystallization under alkaline conditions, and in the presence of phosphate. *American Mineralogist*, 90, 1852–1860.
- Swedlund, P.J. and Webster, J.G. (2001) Cu and Zn ternary surface complex formation with SO₄ on ferrihydrite and schwertmannite. *Applied Geochemistry*, 16, 503–511.
- Towe, K.M. and Bradley, W.F. (1967) Mineralogical constitution of colloidal hydrous ferric oxides. *Journal of Colloid and Interface Science*, 24, 384–392.
- Waychunas, G.A., Xu, N., Fuller, C.C., Davids, J.A., and Bingham, J.M. (1995) XAS study of AsO₄³⁻ and SeO₄²⁻ substituted schwertmannites. *Physica B*, 208 and 209, 481–483.
- Webster, J.G., Swedlund, P.J., and Webster, K.S. (1998) Trace metal adsorption onto an acid mine drainage iron(III) oxy hydroxy sulfate. *Environmental Science and Technology*, 32, 1361–1368.
- Yu, J.Y. and Heo, B. (2001) Dilution and removal of dissolved metals from acid mine drainage along Imgok Creek, Korea. *Applied Geochemistry*, 16, 1041–1053.
- Yu, J.Y., Heo, B., Choi, I.K., Cho, J.P., and Chang, H.W. (1999) Apparent solubilities of schwertmannite and ferrihydrite in natural stream waters polluted by mine drainage. *Geochimica et Cosmochimica Acta*, 63, 3407–3416.
- Yu, J.Y., Park, M., and Kim, J. (2002) Solubilities of synthetic schwertmannite and ferrihydrite. *Geochemical Journal*, 36, 119–132.

MANUSCRIPT RECEIVED AUGUST 7, 2007

MANUSCRIPT ACCEPTED JANUARY 30, 2008

MANUSCRIPT HANDLED BY HONGWU XU